

Effect of Paste Viscosity on Direct-Current Resistance in Improving the Efficiency of Dye-Sensitized Solar Cell

S.N.A.Zaine¹, N.M.Mohamed^{1,2}, M.Khatani³ and M.U.Shahid¹

¹Fundamental and Applied Science Department, Universiti Teknologi PETRONAS,
32610 Bandar Seri Iskandar, Perak, Malaysia.

²Centre of Innovative Nanostructure and Nanodevices (COINN), Universiti Teknologi PETRONAS,
32610 Bandar Seri Iskandar, Perak, Malaysia.

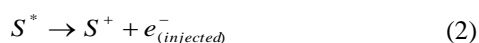
³Electrical and Electronic Department, Universiti Teknologi PETRONAS,
32610 Bandar Seri Iskandar, Perak, Malaysia.
siti.nur_g02580@utp.edu.my

Abstract—The quality of photoelectrode film plays an important role in producing high performing dye-sensitized solar cell (DSC). A well-deposited film would ensure the stability of photoelectrode material and improve electron transport and recombination. This study aims to evaluate the effect of paste viscosity on the direct-current resistance of the fabricated DSC. Photoelectrode paste of different viscosity was prepared by varying the amount of terpeneol as the solvent. Photoelectrode films were then deposited on fluorine-doped tin oxide glass substrate by screen printing method. Electrochemical impedance spectroscopy analysis was utilized to analyse the direct-current resistance of fabricated DSC integrated with different paste viscosity. Direct-current resistance is found to be reduced with increasing paste viscosity. This is attributed to the increase in electron density which reduces the transport as well as recombination resistance leading to an improvement in the conversion efficiency.

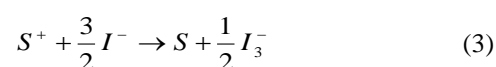
Index Terms—Dye-sensitized Solar Cell; Electrochemical Impedance; Paste Viscosity; Photoelectrode Material, TiO₂ Film.

I. INTRODUCTION

Dye-sensitized solar cell (DSC), also known as Gratzel cell is the third generation solar technology [1-3]. DSC consists of three main parts namely working electrode made up of photoelectrode material coated with dye sensitizer, counter electrode deposited with Pt catalytic film and the redox couple electrolyte. The working principle of DSC is mimicking photosynthesis where the photosensitized dye sensitizer molecules are analogous to chlorophyll of the leave structure. When the sunlight strikes the dye molecules on the surface of TiO₂, the dye molecule (S) absorbs the energy of photon and transform to the excited state (S*). The excitation of the dye is followed by injection of the resulting electrons into the conduction band of the photoelectrode usually TiO₂, leaving dye in the oxidized state (S⁺). This phenomenon can be written in the form of equilibrium reaction as shown in Equation. 1 and 2, where $h\nu$ is the photon energy [1-5].



Electron regeneration of dye sensitizer occurs through electrons donation from iodide/tri-iodide redox electrolyte in contact with the dye as represented in Equation 3.



The injected electrons collected on the working electrode side, travel along the external circuit to power the load and then flow to the counter electrode side. The electrons that reach counter electrode side will reduce the tri-iodide into iodide.

The heart of DSC lies on the photoelectrode semiconductor material which is critical in holding the dye and transporting the electrons. Over the recent years, the developments of mesoscopic oxide or chalcogenide nanoparticles as photoelectrode material in DSC have attracted considerable attention. Several porous oxide semiconductor materials i.e. zinc oxide (ZnO) [6-10], niobium pentoxide (Nb₂O₅) [5, 11], stannous oxide (SnO₂) [12-15] and indium oxide (In₂O₃) [5, 11] have been intensively studied as potential photoelectrode in DSC, however nanocrystalline TiO₂ shows the best performance [5, 11, 16-19]. In addition, TiO₂ also have a good chemical stability, nontoxic, widely available and inexpensive [5]. Other materials such as Si, GaAs, InP and CdS have also been used as photoelectrode material yet decomposed under irradiation thus raising the concern on toxicity [5, 20-22].

The photoelectrode film of TiO₂ can be deposited on conductive substrate through several method namely screen printing, doctor blading, roller coating as well as spray pyrolysis. Amongst them, screen printing is a reasonably low-cost process which can promise reproducibility, high flexibility for pattern printing, high lateral resolution where printed film thickness can be varied over large range. The properties of the photoelectrode paste will determine the quality of the printed photoelectrode film. This study aims to investigate the effect of photoelectrode paste viscosity on the performance of DSC in relation to the direct current resistance. The photoelectrode paste based on TiO₂ was prepared using commercially available TiO₂ nanoparticles. The viscosity of the prepared paste was varied and their effect on the produced photoelectrode film deposited through screen

printing technique was evaluated.

II. METHODOLOGY

Four samples of photoelectrode paste with different viscosity were prepared using commercial TiO₂ purchased from Sigma Aldrich, ethyl cellulose, terpineol, ethanol, water and acetic acid [23-25]. The viscosity of each paste was adjusted using terpineol as solvent so that their ranges are in 10000 cP to 40000 cP. The viscosity was verified using viscometer (CAP 2000+, Brookfield) tested at 25°C. The measurement was taken utilizing spindle number 9. Since the prepared paste samples were non-Newtonian fluid, some differences in the testing parameters were expected. However, all samples were tested at typical testing temperature of 25°C and hold time of 10s.

Each prepared paste was then printed on fluorine-doped tin oxide (FTO) glass substrate to form photoelectrode film with active screen area of 1 cm². Variable pressure field emission scanning electron microscope (Zeiss Supra 55VP, Carl Zeiss) was used to examine the morphology and thickness of printed photoelectrode film. The thickness of printed films was further verified through stylus method using surface roughness tester (SV-3000, Mitutoyo) across the printed photoelectrode film. In the measurement, the tested length was set to be longer than the width of the active area so that the thickness can be estimated based on the difference of the height of surface substrate with the photoelectrode film.

The capability of the printed photoelectrode film to contain dye molecules was measured using UV-Vis spectroscopy (Cary 100, Agilent) of desorbed dye solution from the respective photoelectrode film. In measuring the absorption spectra of desorbed dye solution, the printed photoelectrode films were firstly soaked overnight in N719 dye solution. The dyed photoelectrode films were then rinsed with ethanol and then desorbed in diluted ammonium hydroxide solution to remove the absorbed dye molecules on the surface of photoelectrode film. The solutions were tested for the light absorption in the wavelength range of 200 nm to 800 nm with diluted ammonium solution as reference solution. The loading capacity was calculated based on the average of concentration of dye molecules of at least 3 samples for each prepared viscosity at wavelength of 530.4 nm.

Gamry instruments (PCI4-300) with Echem analyst software of electrochemical impedance spectroscopy (EIS) was utilized to analyse the electrochemical properties of the integrated DSC. The testing parameters such as bias, frequency range, modulation amplitude were set at -0.68V vs. *E_{ref}*, 300 kHz to 0.1 Hz, 10 mV AC with 10 points/decade, respectively. The performance of the integrated DSCs was verified using a Universal Photovoltaic Test System, Dyesol under 1000 W/cm² intensity of illuminant Xenon lamp at an AM-1.5 radiation angle connected to a voltmeter and ampere

meter (Model 2420, Keithly) with variable load. The parameter namely voltage limit, current max, delay, active area and sun level were adjusted to 0.8 V for *V_{max}* and -0.1 V for *V_{min}*, 0.02 A, 0.1 sec, 1.00 cm² and 1 sun level, respectively.

III. RESULT AND DISCUSSION

In order to study the effect of paste viscosity on the performance of TiO₂ photoelectrode film, the prepared TiO₂ pastes were adjusted to four different viscosities using terpineol. Based on the value of Full Scale Range (FSR), the viscosity of the samples and accuracy of the measurement was calculated by considering the cone constant range of 5000 and accuracy of ±2%. The results were tabulated in Table 1 with the FSR at rpm and accuracy of spindle was calculated based on Equation 4 and 5:

$$FSR \text{ at rpm}(P) = \frac{\text{Cone constant range}}{\text{rpm}} \quad (4)$$

$$\text{Accuracy of spindle}(cP) = \pm 2\% \times FSR \text{ at rpm} \times 100 \quad (5)$$

The analysis shows that sample 1 having viscosity in the range of about 10000-12000 cP, sample 2 of about 19000-21000 cP while sample 3 and 4 having viscosity of 28000-31000 cP and 41000-45000 cP, respectively. The prepared pastes were then deposited on FTO substrate using screen printing method.

Figure 1 shows the cross-section images of the printed TiO₂ photoelectrode film taken using FESEM at 2.00 KX magnification. The measurement of the thickness was taken by considering the average high between the peaks and valleys of the printed film. The thickness of printed films was further verified through stylus method and the results were summarized in Table 2. The measured thickness shows that sample 1 with the lowest viscosity exhibited the thinnest photoelectrode film of about 6.2 μm, while sample 2, 3 and 4 exhibited thickness of about 6.3 μm, 6.4 μm and 6.6 μm, respectively. Based on the analysis, it is clear that the increase of the viscosity to approximately 10000 cP will result in an increase of photoelectrode film to about 0.1-0.2 μm.

Table 2
Thickness of Photoelectrode film measured using FESEM and Stylus Method

Paste Sample	Average thickness estimated using FESEM (μm)	Average Thickness estimated by stylus (μm)
1	6.145	6.209
2	6.384	6.319
3	6.462	6.416
4	6.615	6.577

Table 1
Samples of Prepared Photoelectrode Paste at Different Viscosity

Paste Sample	Run time (s)	Speed (rpm)	Sheer rate (s)	Measured Viscosity (cP)	% FSR	FSR at rpm (P)	Accuracy of spindle (cP)	Sample viscosity (cP)
1	120	18	36	11757	96.2	277.78	556	11310 ±556
2	25	10	20	21406	97.3	500.00	1000	20828 ±1000
3	80	7	14	30360	96.6	714.29	1429	29328 ±1429
4	30	5	10	43560	99.0	1000.00	2000	43124 ±2000

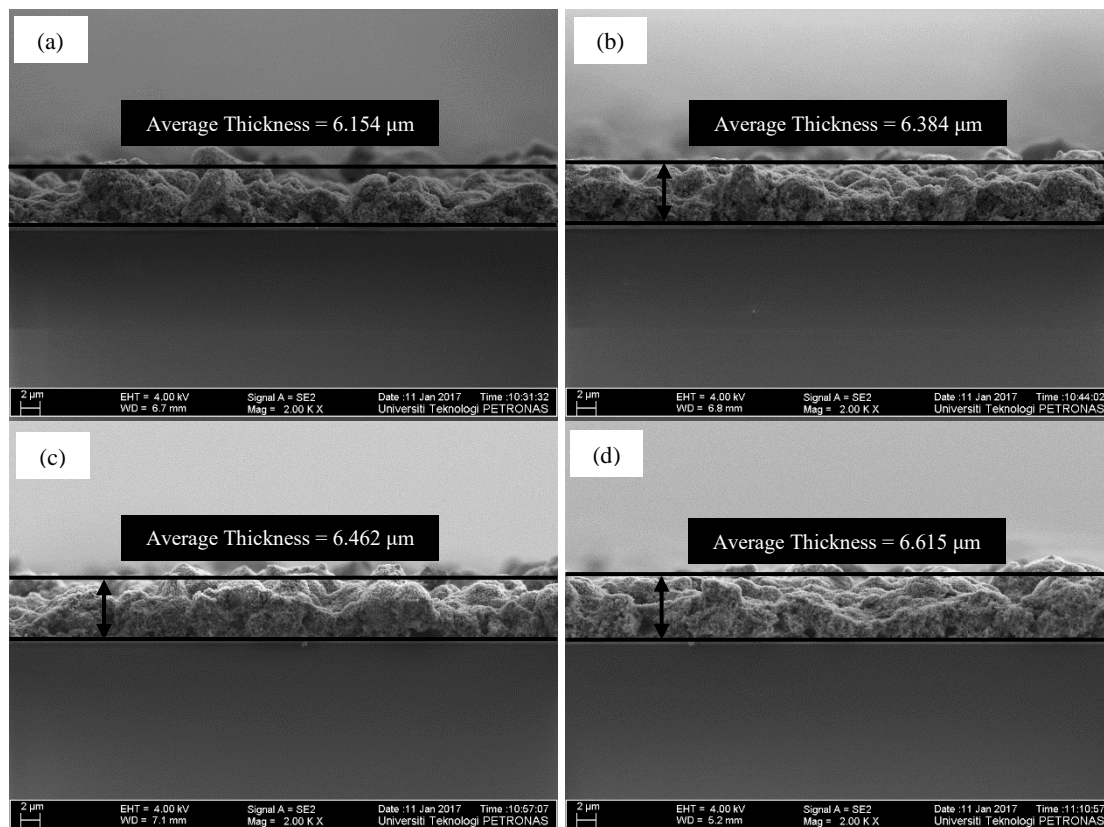


Figure 1: Cross-section FESEM images of the photoelectrode films printed on FTO substrate using paste with different viscosity of (a) sample 1, (b) sample 2, (c) sample 3 and (d) sample 4

The capability of photoelectrode film to anchor dye molecules was verified through UV-Vis spectroscopy analysis. Figure 2 shows the spectra of desorbed N719 dye in diluted ammonium hydroxide solution. In addition, absorption spectrum of TiO_2 is also included as comparison. The spectra of all desorbed dye samples have peaks appeared at wavelengths of 310 nm, 372 nm and 509 nm, corresponding to ligand-centred charge transfer (LCCT) transitions ($\pi-\pi^*$) and metal-to-ligand charge transfer (MLCT) transitions ($4d-\pi^*$) [9, 26, 27] of N719 dye. The spectra show that increase the viscosity of the prepared paste results in increasing the absorption intensity, corresponding to the increase of the amount of anchored dye molecules.

The dye loading capability per square centimetre of printed photoelectrode films was calculated by considering the absorption intensity at wavelength of 530.4 nm. Three samples were tested for each viscosity and the average amount of absorbed dye molecules per square centimetre were tabulated in Table 3. Photoelectrode paste of sample 1, 2, 3 and 4 recorded average amount of absorbed dye of 21.7 μg , 24.4 μg , 26.2 μg and 29.1 μg , respectively. The result shows that there was slight increment in the average amount of absorbed dye when higher viscosity paste was used to prepare the photoelectrode film. This is due to the slight increase in the thickness of photoelectrode film with respect to the increase of the paste viscosity. Besides, photoelectrode paste with higher viscosity results in formation of compact photoelectrode film owing to high density of TiO_2 . This condition leads to the presence of higher surface area by which increase the dye absorption capability.

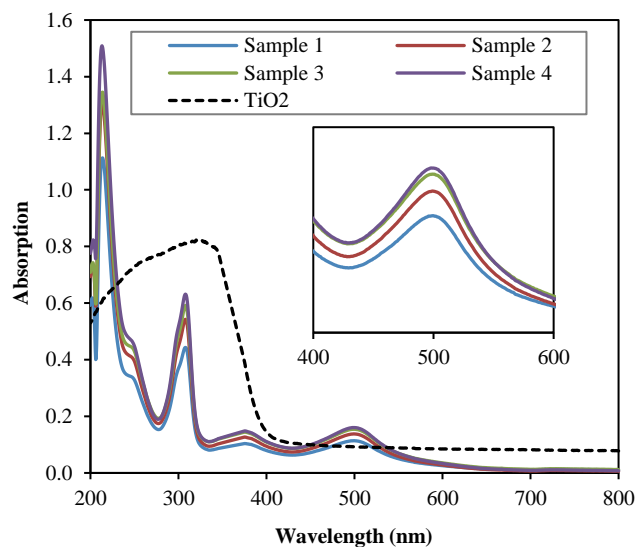


Figure 2: Absorption spectra of desorbed dye solution from photoelectrode TiO_2 films of different paste viscosity

Table 3
Amount of Dye Absorbed per Square Centimetre of Printed Photoelectrode Films of Different Paste Viscosity

Paste Sample	Absorption	Concentration (mM)	Dye absorbed (μg)	Average dye absorbed (μg)
1	0.0244	0.0018	21.7	21.7
2	0.0270	0.0021	24.3	24.4
3	0.0289	0.0022	26.2	26.2
4	0.0318	0.0025	29.1	29.1

In order to study the correlation between the viscosities of the paste with the direct current resistance, the printed photoelectrode films were integrated with Pt counter electrode and iodide/tri-iodide electrolyte. The fabricated cells were then analysed using electrochemical impedance spectroscopy analysis. Figure 3 shows the Nyquist plot of the integrated DSC. The Nyquist plots were fitted based on the transmission line model [28-31] by which made up of resistors and capacitors, as of the insert of Figure 3. R_s of the equivalent circuit represent sheet resistance of substrate and the contact resistance between the substrate and photoelectrode film. R_t and CPE_1 represent the resistance and constant phase element of capacitance related to the electrons transport within the mesoporous photoelectrode network, R_t and the resistance related to recombination at the photoelectrode/dye/electrolyte interface, R_{br} . While, R_2 and CPE_2 represent the resistance and constant phase element of capacitance of charge transfer resistance at counter electrode. R_1 and CPE_1 correspond to the large semicircle while R_2 and CPE_2 correspond to the small semicircle at high frequency range of the Nyquist plot.

Table 4 summarizes the analysed properties such as transport resistance (R_t), recombination resistance (R_{br}), direct-current resistance (R_{dc}), chemical capacitance (C_μ), electron lifetime (τ_n), reaction rate constant for recombination (k), electrons diffusion coefficient (D_n) and steady-state electron density in the conduction band (n_s). The R_{br} was estimated from the diameter of the large semicircle while the transport resistance (R_t) was dependent on the shape of the arc. The k is the inverse of electron lifetime which was estimated from the product of R_{br} and C_μ . The R_{dc} , D_n and n_s were calculated based on Eqn. 6, 7 and 8 [32], respectively.

$$R_{dc} = \frac{1}{3}R_t + R_{br} \quad (6)$$

$$D_n = (R_t C_\mu)^{-1} \quad (7)$$

$$R_{br} = \frac{k_B T}{q^2 A n_s} \cdot \frac{1}{L k_n} = Con \frac{1}{L k_n} \text{ or } R_t = Con \frac{L}{D_n} \quad (8)$$

where: k_B = Boltzmann constant ($1.38 \times 10^{-23} \text{ J.K}^{-1}$)
 T = absolute temperature (298.15 K)
 q = charge of a proton ($1.60 \times 10^{-19} \text{ C}$)
 L = thickness of photoelectrode film
 A = active area of electrode, respectively.

The analysis shows that the measured electrochemical properties are insignificantly affected by the viscosity of the paste except for transport and recombination resistance as well as steady-state electron density in the conduction band

of photoelectrode material. Both R_t and R_{br} are reduced while the n_s is increased as increasing the viscosity of the photoelectrode paste. However, the ratio of R_{br} to R_t represents the favourable of photogenerated electrons to be transported out instead of recombined with the iodide/tri-iodide or oxidized dye molecules is almost same for all samples. This indicates that altering the viscosity of the paste has no significant effect on the electron transport properties of integrated DSC.

Reducing both R_t and R_{br} lead to reduce direct current resistance, R_{dc} . One possible reason is due to the increase in electrons density in the conduction band of TiO_2 [32]. Increase the viscosity of photoelectrode paste would result in slightly increases of the photoelectrode thickness. Besides, a high viscosity paste which contains less amount of terpineol as solvent results in denser photoelectrode TiO_2 film produced. Close packing of TiO_2 film helps in reducing voids, increasing the surface area for dye absorption thus improve the generation of excited electrons. This condition leads to increase the number of excited dye, generating large amount of electrons thus increase the number of injected electrons into the conduction band of TiO_2 .

To evaluate the performance of integrated DSC, test cells with active area of 1 cm^2 was tested under illumination of 1000 W/cm^2 intensity of light simulator. Figure 4 shows the plotted I - V curve of the tested DSC while Table 5 summarized the measured data of the photovoltaic properties. Based on the results, increasing the viscosity of the prepared paste would results in increasing the short-circuit current, thus increasing the performance efficiency of the integrated DSC. The highest performance of DSC was recorded by the photoelectrode film prepared using the thickest photoelectrode paste (sample 4).

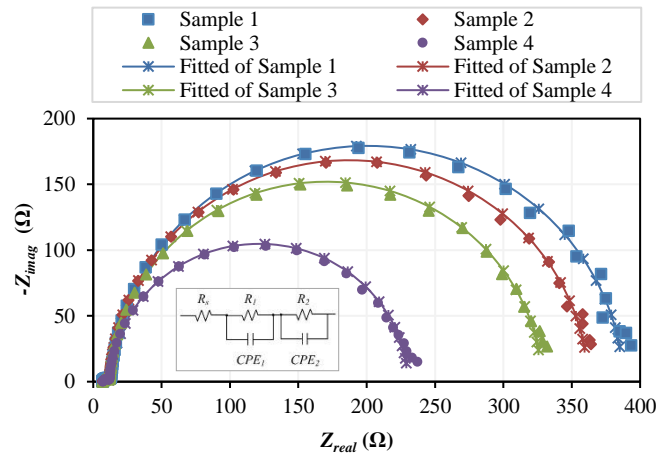


Figure 3: Nyquist plot and equivalent circuit of the DSC integrated with photoelectrode TiO_2 film of different viscosity

Table 4
 The Electrochemical Properties of DSC Integrated with Photoelectrode TiO_2 Film of Different Viscosity

Sample	R_t (Ω)	R_{br} (Ω)	R_{dc} (Ω)	C_μ (F)	τ_n (s)	k (s^{-1})	D_n ($\text{cm}^2 \cdot \text{s}^{-1}$)	Con ($\Omega \cdot \text{cm} \cdot \text{s}^{-1}$)	n_s (cm^{-3})
1	6.92	375.0	377.3	3.15×10^{-4}	0.118	8.458	4.59×10^{-6}	1.9467	0.82×10^{17}
2	5.85	350.2	352.2	3.55×10^{-4}	0.124	8.048	4.81×10^{-6}	1.8024	0.89×10^{17}
3	5.28	292.8	294.6	4.07×10^{-4}	0.119	8.400	4.66×10^{-6}	1.5853	1.01×10^{17}
4	4.03	218.6	219.9	4.94×10^{-4}	0.108	9.258	5.02×10^{-6}	1.3311	1.20×10^{17}

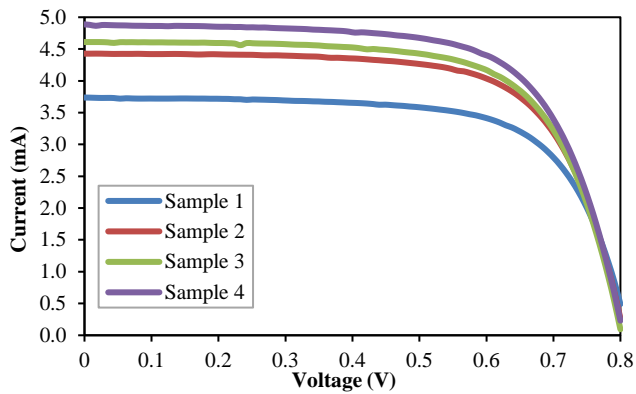


Figure 4: *I-V* curve of DSC integrated with photoelectrode paste of different viscosity

Table 5
Photovoltaic Properties of the Fabricated DSC Integrated with Photoelectrode Paste of Different Viscosity

Paste Sample	I_{sc} (mA)	V_{oc} (V)	FF	η (%)
1	3.738	0.80	0.697	2.085
2	4.428	0.80	0.691	2.447
3	4.610	0.80	0.684	2.521
4	4.888	0.80	0.681	2.663

Regardless of paste viscosity, all tested samples exhibit constant value of open-circuit voltage, V_{oc} (0.8 V). The V_{oc} is proportional to the difference between the Fermi level of the photoelectrode TiO_2 and the electrochemical potential of the redox couple electrolyte [19, 33]. It is expected that there is no changes in the Fermi level of TiO_2 as well as the redox couple potential as the same photoelectrode TiO_2 and iodide/tri-iodide electrolyte were used throughout this study. Besides, V_{oc} is also dependent on the recombination of generated electrons in the conduction band of TiO_2 . The result of V_{oc} is in good agreement with the insignificant difference of the effective rate of recombination with varying viscosity of the prepared paste. The finding indicates that the viscosity of the paste would not affect the electrons recombination process.

However, there is a slight decrease of fill factor, FF with increasing viscosity of the photoelectrode paste. The FF is defined as the ratio of the maximum power ($P_{max} = I_{max} \times V_{max}$) obtained by the device and the theoretical maximum power (P_{th}), where $P_{th} = I_{sc} \times V_{oc}$. It reflects the losses of electrical and electrochemical which is associated with the electron transfer process and internal resistance of a DSC [33]. The decrease in FF is associated to the slight decrease of the recombination resistance as evident in the EIS analysis. This is due to the increase of the photoelectrode thickness with increase of paste viscosity.

Significant changes can be seen for the short-circuit current, I_{sc} of fabricated DSC where it shows an increasing trend. The increase is due to the increase of dye absorption capability of the films resulting in the reducing of the direct current resistance. Large amount of dye molecules anchored by the photoelectrode film prepared using high viscosity paste would increase the number of photogenerated electrons. Thus, small resistance to direct current will ensure that the generated electrons are easily transported within the photoelectrode network and efficiently collected at the conductive substrate of working electrode side.

IV. CONCLUSION

Based on the study of the effect of paste viscosity on the performance of DSC, it is verified that the viscosity of the paste can influence the thickness of printed photoelectrode films. The more viscous the paste, the thicker the photoelectrode film produced. Besides, photoelectrode paste with high viscosity also produce photoelectrode film with less voids, leading to the presence of large specific surface area, thus more dye molecules can be anchored. High amount of anchored dye molecules helps to generate more excited electrons, hence results in improving the amount of steady-state electrons density in the conduction band of TiO_2 . Increase the electron density leads to reduce the value of R_t and R_{br} , thus reduce the R_{dc} .

However, the viscosity of photoelectrode paste has an insignificant effect on the electrons transport properties of the fabricated DSC. The increase of recombination resistance as reducing the paste viscosity was related to the reducing of the thickness of photoelectrode film. Based on this study, it can be concluded that the viscosity of photoelectrode film can be tailored in order to produce the desired thickness of photoelectrode film without compromising the electrochemical properties.

ACKNOWLEDGMENT

The author would like to acknowledge Universiti Teknologi PETRONAS for the financial support and Centralized Analytical Laboratory (CAL) of Universiti Teknologi PETRONAS for the FESEM characterization analysis.

REFERENCES

- [1] B. O. Regan and M. Grätzel, "A low-cost, high efficiency solar cell based on dye-sensitized colloidal TiO_2 films," *Nature*, vol. 353, pp. 737-746, 1991.
- [2] M. Grätzel, "Solar energy conversion by dye-sensitized photovoltaic cells," *Inorganic chemistry*, vol. 44, pp. 6841-6851, 2005.
- [3] M. K. Nazeeruddin, E. Baranoff, and M. Grätzel, "Dye-sensitized solar cells: A brief overview," *Solar Energy*, vol. 85, pp. 1172-1178, 2011.
- [4] M. Shakeel Ahmad, A. K. Pandey, and N. Abd Rahim, "Advancements in the development of TiO_2 photoanodes and its fabrication methods for dye sensitized solar cell (DSSC) applications: A review," *Renewable and Sustainable Energy Reviews*, vol. 77, pp. 89-108, 2017.
- [5] K. Hara and H. Arakawa, "Dye-sensitized solar cells," in *Handbook of Photovoltaic Science and Engineering*, A. Luque and S. Hegedus, Eds., ed: John Wiley & Sons, 2003, pp. 663-699.
- [6] S. Yun, J. Lee, J. Chung, and S. Lim, "Improvement of ZnO nanorod-based dye-sensitized solar cell efficiency by Al-doping," *Journal of Physics and Chemistry of Solids*, vol. 71, pp. 1724-1731, 2010.
- [7] Q. F. Zhang, C. S. Dandeneau, X. Y. Zhou, and G. Z. Cao, "ZnO nanostructures for dye-sensitized solar cells," *Adv. Mater.*, vol. 19, pp. 4087-4108, 2009.
- [8] Q. Zhang, T. P. Chou, B. Russo, S. A. Jenekhe, and G. Cao, "Polydisperse aggregates of ZnO nanocrystallites: A method for energy-conversion-efficiency enhancement in dye-sensitized solar cells," *Advanced Functional Materials*, vol. 18, pp. 1654-1660, 2008.
- [9] Q. Zhang, T. P. Chou, B. Russo, S. A. Jenekhe, and G. Cao, "Aggregation of ZnO nanocrystallites for high conversion efficiency in dye-sensitized solar cells," *Angewandte Chemie International Edition*, vol. 47, pp. 2402-2406, 2008.
- [10] T. P. Chou, Q. Zhang, G. E. Fryxell, and G. Cao, "Hierarchically structured ZnO film for dye-sensitized solar cells with enhanced energy conversion efficiency," *Adv. Mater.*, vol. 19, pp. 2588-2592, 2007.
- [11] B. A. Gregg, "Excitonic solar cells," *J. Phys. Chem. B*, vol. 107, pp. 4688-4698, 2003.
- [12] C. S. K. Ranasinghe, E. N. Jayaweera, G. R. A. Kumara, R. M. G. Rajapakse, B. Onwona-Agyeman, A. G. U. Perera, et al., "Tin oxide based dye-sensitized solid-state solar cells: surface passivation for

- suppression of recombination," *Materials Science in Semiconductor Processing*, vol. 40, pp. 890-895, 2015.
- [13] Y. J. Kim, K. H. Kim, P. Kang, H. J. Kim, Y. S. Choi, and W. I. Lee, "Effect of layer-by-layer assembled SnO₂ interfacial layers in photovoltaic properties of dye-sensitized solar cells," *Langmuir*, vol. 28, pp. 10620-10626, 2012.
- [14] J. Qian, P. Liu, Y. Xiao, Y. Jiang, Y. Cao, X. Ai, et al., "TiO₂-coated multilayered SnO₂ hollow microspheres for dye-sensitized solar cells," *Adv. Mater.*, vol. 21, pp. 3663-3667, 2009.
- [15] R. R. Knauf, B. Kalanyan, G. N. Parsons, and J. L. Dempsey, "Charge recombination dynamics in sensitized SnO₂/TiO₂ core/shell photoanodes," *The Journal of Physical Chemistry C*, vol. 119, pp. 28353-28360, 2015.
- [16] S. Mathew, A. Yella, P. Gao, R. Humphry-Baker, F. E. Curchod Basile, N. Ashari-Astani, et al., "Dye-sensitized solar cells with 13% efficiency achieved through the molecular engineering of porphyrin sensitizers," *Nat. Chem.*, vol. 6, pp. 242-247, 2014.
- [17] Y. Chiba, A. Islam, Y. Watanabe, R. Komiya, N. Koide, and L. Han, "Dye-sensitized solar cells with conversion efficiency of 11.1%," *Japanese Journal of Applied Physics*, vol. 45, p. L638, 2006.
- [18] Y. Cao, Y. Saygili, A. Ummadisingu, J. Teuscher, J. Luo, N. Pellet, et al., "11% efficiency solid-state dye-sensitized solar cells with copper (II/I) hole transport materials," *Nature Communication*, vol. 8, pp. 1-8, 2017.
- [19] R. Jose, V. Thavasi, and S. Ramakrishna, "Metal oxide for dye-sensitized solar cells," *Journal of American Ceramic Society*, vol. 92, pp. 289-301, 2009.
- [20] F. Huang, J. Hou, Q. Zhang, Y. Wang, R. C. Massé, S. Peng, et al., "Doubling the power conversion efficiency in CdS/CdSe quantum dot sensitized solar cells with a ZnSe passivation layer," *Nano Energy*, vol. 26, pp. 114-122, 2016.
- [21] A. Manjceevan and J. Bandara, "Robust surface passivation of trap sites in PbS q-dots by controlling the thickness of CdS layers in PbS/CdS quantum dot solar cells," *Solar Energy Materials and Solar Cells*, vol. 147, pp. 157-163, 2016.
- [22] Z. Chen and Y.-J. Xu, "Ultrathin TiO₂ layer coated-CdS spheres core-shell nanocomposite with enhanced visible-light photoactivity," *ACS Applied Materials & Interfaces*, vol. 5, pp. 13353-13363, 2013.
- [23] S. Ito, "How to make high-efficiency dye-sensitized solar cells," in *Dye-sensitized Solar Cells*, K. Kalyanasundaram, Ed., ed Switzerland: EPFL Press, 2010, pp. 251-266.
- [24] S. Ito, T. N. Murakami, P. Comte, P. Liska, C. Grätzel, M. K. Nazeeruddin, et al., "Fabrication of thin film dye sensitized solar cells with solar to electric power conversion efficiency over 10%," *Thin Solid Films*, vol. 516, pp. 4613-4619, 2008.
- [25] S. Ito, P. Chen, P. Comte, M. K. Nazeeruddin, P. Liska, P. Pechy, et al., "Fabrication of screen-printing pastes from TiO₂ powders for dye-sensitized solar cells," *Progress in Photovoltaics: Research and Applications*, vol. 15, pp. 603-612, 2007.
- [26] S. Agarwala, M. Kevin, A. S. W. Wong, C. K. N. Peh, V. Thavasi, and G. W. Ho, "Mesophase ordering of TiO₂ film with high surface area and strong light harvesting for dye-sensitized solar cell," *ACS Applied Materials & Interfaces*, vol. 2, pp. 1844-1850, 2010.
- [27] B. Basheer, D. Mathew, B. K. George, and C. P. Reghunadhan Nair, "An overview on the spectrum of sensitizers: The heart of dye sensitized solar cells," *Solar Energy*, vol. 108, pp. 479-507, 2014.
- [28] J. Bisquert and I. Mora-Sero, "Simulation of steady-state characteristics of dye-sensitized solar cells and the interpretation of the diffusion length," *J. Phys. Chem. Lett.*, vol. 1, pp. 450-456, 2010.
- [29] Q. Wang, S. Ito, M. Gratzel, F. Fabregat-Santiago, I. n. Mora-Sero, J. Bisquert, et al., "Characteristics of high efficiency dye-sensitized solar cells," *J. Phys. Chem. B* vol. 110, pp. 25210-25221, 2006.
- [30] J. Bisquert, A. Zaban, M. Greenshtein, and I. Mora-Seró, "Determination of rate constants for charge transfer and the distribution of semiconductor and electrolyte electronic energy levels in dye-sensitized solar cells by open-circuit photovoltage decay method," *J. Am. Ceram. Soc.*, vol. 126, pp. 13550-13559, 2004.
- [31] J. Bisquert, "Theory of the impedance of electron diffusion and recombination in a thin layer," *J. Phys. Chem. B*, vol. 106, pp. 325-333, 2002.
- [32] M. Adachi, M. Sakamoto, J. Jiu, Y. Ogata, and S. Isoda, "Determination of parameters of electron transport in dye-sensitized solar cells using electrochemical impedance spectroscopy," *J. Phys. Chem. B*, vol. 110, pp. 13872-13880, 2006.
- [33] S. Zhang, X. Yang, Y. Numata, and L. Han, "Highly efficient dye-sensitized solar cells: progress and future challenges," *Energy Environment Science*, vol. 6, pp. 1443-1464, 2013.